Interactive Retinal Vessel Centreline Extraction and Boundary Delineation using Anisotropic Fast Marching and Intensities Consistency

Da Chen and Laurent D. Cohen

Abstract— **In this paper, we propose a new interactive retinal vessels extraction method with anisotropic fast marching (AFM) based on the observation that one vessel may have the property of local intensities consistency. Our goal is to extract both the centrelines and boundaries between two given points. The proposed method consists of two stages: the first stage aims to finding the vessel centrelines using AFM and local intensities consistency roughly, while the second stage is to refine the centrelines from the previous stage using constrained Riemannian metric based AFM, and get the boundaries of the vessels simultaneously. Experiments show that results of our method outperform the classical minimal path method [1].**

I. Introduction

Retinal vessel extraction is a crucial task in retinal disease diagnostics such as retinopathy of prematurity. However, it remains a challenge to extract the accurate vessels interactively from the retinal image due to its complex vessel topological structure, low contrast grey level and noise. Geodesic or minimal path methods have been successfully applied to line or tubular patterns extraction in various computer vision and medical imaging tasks [2] since the seminal work by Cohen and Kimmel [3], in which tubular structures, or object edges are extracted as the form of geodesics or minimal paths. This classic minimal path model can lead to finding the global minimum with respect to a geodesic energy potential $\mathcal{P}$ between two given endpoints. The geodesic potential or metric can be isotropic [3] ($\mathcal{P}$ only depends on the pixel position), or anisotropic in the sense that path length depends on the path orientation as well [1]. Once this potential is properly defined, Fast Marching (FM) methods [4] [5] are the favoured methods to estimate geodesic distances, from which minimal paths can be extracted.

Unfortunately, for the minimal path models mentioned above, it is difficult to extract the centreline of the tubular structure and the local width information or boundaries simultaneously. In order to solve this drawback, Li and Yezzi [6] proposed a variant minimal path technique, which defines the potential domain $\mathbf{\Omega} \in R^{n+1}$, connected open and bounded, as the product of spatial space $\Omega \in R^n$ with a parameter space $]R_{min}, R_{max}[$ denoting the vessel radius dimension. Thus, each point in the extracted path by[6] contains spatial position and the last dimension represents the vessel thickness at this spatial point. Benmansour and Cohen [1] proposed to use an anisotropic Riemannian metric to avoid shortcuts problem suffered by the Li-Yezzi model. In [1], the authors construct a multi-resolution Riemannian metric guiding the AFM propagation in the domain $\mathbf{\Omega}$.

Da Chen and Laurent D. Cohen are with CEREMADE, Université Paris Dauphine PSL⋆, France. chenda@ceremade.dauphine.fr

For the interactive retinal vessel extraction, the anisotropic Benmansour-Cohen (B-C) model [1] will suffer from *short branches combination* problem(see Section II-C). Wei et al. [7] proposed a curvature constrained FM method to overcome this *short branches combination* problem. In [7] the authors detect the curvature for each pixel in the FM front. If the curvature of a pixel is larger than the given threshold, this pixel will be frozen. However, this model can only extract the centrelines of the vessels and heavily rely on the curvature threshold.

In this paper, we propose a new minimal path based retinal vessel extraction method. Our method is motivated by the fact that the vessel may have local intensities consistency especially for the vessels starting from the retinal optic disk. Instead of using the grey level to compute the local intensities consistency, we utilize the *vesselness* map calculated by the image gradient. The proposed method can be divided into two stages: in the first stage we construct a dynamic Riemannian metric combining the vessel anisotropy and local intensities consistency penalty. With the AFM, the rough centreline of the vessel can be extracted avoiding the *short branches combination* problem even for a long vessel. In the second stage, the extracted centreline is taken as prior path and a Riemannian metric in $\mathbf{\Omega}$ with distance function defined by the prior centreline is constructed.

The paper is organized as follows: in Section II, we briefly introduce the minimal path, oriented flux based Riemannian metric construction, AFM as well as the limitations of the B-C model. In Section III we give details of the proposed method. Experiments are shown in Section IV.

II. Background

In this paper, we only consider the 2D vessel segmentation so that one point $\mathbf{x} = (\hat{x}, r) \in \Omega \subseteq \mathbb{R}^2 \times]R_{min}, R_{max}[$, where $\hat{x} \in \hat{\Omega}$ ($\hat{\Omega} \subset \mathbb{R}^2$) denotes the point position in spatial dimensions and $r \in \ ]R_{min}, R_{max}[$ denotes the position in radius dimension.

A. Minimal Path

Let $\Im$ denote the collection of Lipschitz paths $\gamma : \ [0, L] \to \Omega$. The weighted length through a geodesic energy potential $\mathcal{P}$ can be formulated as follows:

$$l_{\mathcal{P}}(\gamma) := \int_0^L \mathcal{P}(\gamma(s), \gamma'(s)) \ ds \tag{1}$$

where $\mathbf{p}$ is arc-length parameter and γ' denotes the tangent vector of path γ. The geodesic distance $\mathcal{U}_{\mathbf{p}}(\mathbf{x})$, or minimal action map, is the minimal energy of any path joining a point $\mathbf{x} \in \Omega$ to a given initial point $\mathbf{p}$:

$$\mathcal{U}_{\mathbf{p}}(\mathbf{x}) := \min\{l_{\mathcal{P}}(\gamma) | \gamma \in \Im,\ \gamma(L) = \mathbf{x},\ \gamma(0) = \mathbf{p}\}. \quad (2)$$

The path $\mathcal{C}_{\mathbf{p},\mathbf{x}}$ is called a minimal path if $l_{\mathcal{P}}(\mathcal{C}_{\mathbf{p},\mathbf{x}}) = \min_{\gamma}\{l_{\mathcal{P}}(\gamma) |\ \gamma \in \Im\}$.

B. Riemannian Metric Construction

In this paper we utilize the optimal oriented flux [8] to construct the Riemannian metric. The oriented flux of a given image $I : \hat{\Omega} \to \mathbb{R}^2$, of dimension 2, is defined as the amount of the image gradient projected along the orientation $\vec{p}$ flowing out from a 2D circle at point x with radius r:

$$f(\hat{x}; r, \vec{p}) = \int_{\partial \mathcal{C}_r} (\nabla(G_\sigma * I)(\hat{x} + r\vec{p}) \cdot \vec{p})(\vec{p} \cdot \vec{n}) ds \quad (3)$$

where G_σ is a Gaussian with variance σ and $\vec{n}$ is the outward unit normal vector along $\partial \mathcal{C}_r$. ds is the infinitesimal length on the boundary of $\mathcal{C}_r$. According to the divergence theory, one has $f(\hat{x}; r, \vec{p}) = \vec{p}^T \cdot \mathbf{Q}(x, r) \cdot \vec{p}$ for some symmetric matrix $\mathbf{Q}(x, r)$ whose eigenvalues and eigenvectors we denote by λ_i and $\mathbf{v}_i$, $i = 1, 2$ (Suppose $\lambda_1 \leq \lambda_2$). The symmetric matrix $\mathbf{Q}(x, r)$ is defined by the oriented flux filter $\mathbf{F}_r$ as:

$$\mathbf{Q}(x, r) = \Big(I * (\mathbf{F}_r \cdot \frac{1}{r})\Big)(x, r) \quad (4)$$

In this paper, the potential $\mathcal{P}(\gamma, \gamma')$ is set as a quadratic form with respect to a symmetric positive definite tensor $\mathcal{M}$ which is a 3×3 symmetric matrix:

$$\mathcal{P}(\gamma, \gamma') = \sqrt{\gamma'(.)^T \mathcal{M}(\gamma(.)) \gamma'(.)}\ . \quad (5)$$

As described in [1], we consider the anisotropy only in the spatial dimensions. Thus $\mathcal{M}$ can be decomposed as follows:

$$\mathcal{M}(x, r) = \begin{pmatrix} \tilde{\mathcal{M}}(x, r) & \mathbf{0} \\ \mathbf{0} & \mathcal{P}_r(x, r) \end{pmatrix}. \quad (6)$$

The anisotropic entry $\tilde{\mathcal{M}}(x, r)$, which is a 2×2 symmetric definite positive matrix, at point $\mathbf{x} = (x, r)$ can be constructed by the uint orientation vectors $\mathbf{v}_1$ and $\mathbf{v}_2$ as:

$$\tilde{\mathcal{M}}(\mathbf{x}) = e^{\alpha \cdot \lambda_2(\mathbf{x})} \mathbf{v}_1(\mathbf{x}) \mathbf{v}_1(\mathbf{x})^T + e^{\alpha \cdot \lambda_1(\mathbf{x})} \mathbf{v}_2(\mathbf{x}) \mathbf{v}_2(\mathbf{x})^T, \quad (7)$$

The isotropic entry $\mathcal{P}_r(\mathbf{x})$ can be computed as:

$$\mathcal{P}_r(\mathbf{x}) = \beta \exp\Big(\alpha \frac{\lambda_1(\mathbf{x}) + \lambda_2(\mathbf{x})}{2}\Big), \quad (8)$$

where α controls the spatial anisotropic ratio defined as

$$\mu = \max_{(\hat{x}, r) \in \mathbf{\Omega}} \sqrt{\exp\left(\alpha \cdot (\lambda_2(\hat{x}, r) - \lambda_1(\hat{x}, r))\right)}$$

while β controls the radius speed. For in-depth details we refer to [1]. The minimal action map $\mathcal{U}_{\mathbf{p}}(\mathbf{x})$ can be solved by AFM efficiently, which is a one-pass solver for the Eikonal equation:

$$\|\nabla \mathcal{U}_{\mathbf{p}}(\mathbf{x})\|_{\mathcal{M}^{-1}} = 1, \quad \mathcal{U}_{\mathbf{p}}(\mathbf{p}) = 0. \quad (9)$$

The FM methods for the minimal action map $\mathcal{U}_{\mathbf{p}}(\mathbf{x})$, satisfying (9), introduce a discretization grid Z of Ω, and

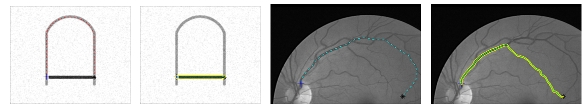

(a) (b) (c) (d)

Fig. 1. Results from the B-C model [1]. (a) and (c) are original images with initial point labeled as '+' and endpoint labeled as '$*$'. the cyan dashed lines indicate the desired paths. (b) and (d) are wrong results of [1].

for each $\mathbf{x} \in Z$ a small mesh $S(\mathbf{x})$ of a neighborhood of $\mathbf{x}$ with vertices in Z (with the adequate modification if $\mathbf{x}$ is at or near the boundary). An approximation of $\mathcal{U}_{\mathbf{p}}$ is given by the solution of the following fixed point problem [5]: find $\mathcal{U}_{\mathbf{p}} : Z \to \mathbb{R}$ such that (i) $\mathcal{U}_{\mathbf{p}}(\mathbf{p}) = 0$ for the initial point $\mathbf{p}$, and (ii) for all $\mathbf{x} \in Z \setminus \mathbf{p}$

$$\mathcal{U}_{\mathbf{p}}(\mathbf{x}) = \min_{\mathbf{y} \in \partial S(\mathbf{x})} \mathcal{P}(\mathbf{x}, \mathbf{y} - \mathbf{x}) + I_{S(\mathbf{x})} \mathcal{U}_{\mathbf{p}}(\mathbf{y}), \quad (10)$$

where $I_{S(\mathbf{x})}$ denotes piecewise linear interpolation on a mesh $S(\mathbf{x})$. $I_{S(\mathbf{x})}$ interpolates $\mathcal{U}_{\mathbf{p}}$ on $S(\mathbf{x})$ [1], [5], [9].

C. Limitations of B-C Model In Retinal Vessels Extraction

The B-C model [1] minimizes the geodesic energy functional formulated in (1) to obtain the minimal action map $\mathcal{U}$ as defined in (2). Though this model has many advantages, such as getting the centrelines and boundaries of tubular structures simultaneously, easy incorporation of user intervention and fast implementation, it may fall into failures due to the *short branches combination*, when extracting tubular structures crossing each other that are very common in retinal vessel network.

In Fig. 1(b) and (d), the extracted path (green line) by B-C model misses the desired vessel. Those mistakes are mainly caused by the fact that the FM propagation with the metric defined by Φ in (5) favours to choose a path with minimal arrival time instead of the desired path. As shown in Fig. 1(b) and (d), combining wrong bifurcations may have smaller arrival time than combining the *desired vessel segments*. In order to overcome this problem, we propose a new minimal path method combining the vessel local intensities consistency. With the local intensities consistency penalty, the speed function is dynamically updated while maintaining the vessel anisotropy.

III. Proposed Method

The proposed method can be divided into two stages: 1) roughly centrelines extraction with dynamic Riemannian metric and 2D AFM. 2) Final centrelines and boundaries extraction based on the results from the first stage and 2D+radius AFM.

A. Retinal Vessel Centrelines Extraction by Intensities Consistency and dynamic Riemannian Metric

We define the 2D Riemannian metric $\tilde{\mathcal{M}}_d$ using the optimal oriented flux [8] and intensities consistency as follows:

$$\tilde{\mathcal{M}}_d(\hat{x}) = (H \cdot (e^{\tau \tilde{\lambda}_2} \tilde{\mathbf{v}}_1 \tilde{\mathbf{v}}_1^T + e^{\tau \tilde{\lambda}_1} \tilde{\mathbf{v}}_2 \tilde{\mathbf{v}}_2^T))(\hat{x}), \quad (11)$$

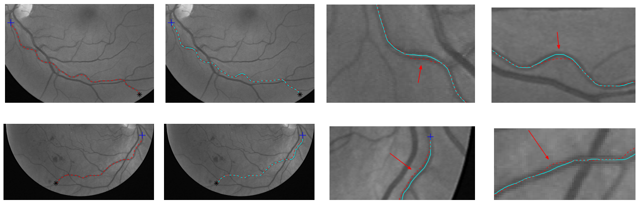

Fig. 2. Centreline bias from the first stage(see text).

where $\hat{x} \in \hat{\Omega} \subset \mathbb{R}^2$ and τ controls the anisotropic ratio. H is the penalty of intensities consistency:

$$H(\hat{x}) = H_d(\hat{x}) + H_c(\hat{x}), \tag{12}$$

In order to define $\tilde{\lambda}_1, \tilde{\lambda}_2, \tilde{\mathbf{v}}_1, \tilde{\mathbf{v}}_2, H_d$ and H_c, we firstly introduce the optimal oriented flux [8] based *vesselness* V_{ness}. Recall that λ_1 and λ_2 are the two eigenvalues of $\mathbf{Q}$ presented in (4) and for retinal vessels, one has $\lambda_2(\hat{x}, \cdot) \gg \lambda_1(\hat{x}, \cdot) \approx 0$ if $\hat{x}$ is inside the vessels. The *Vesselness* V_{ness} and optimal scale map V_{scale} can be defined as:

$$V_{ness}(\hat{x}) = \max_r \Big\{\lambda_2(\hat{x}, r)\Big\}, \tag{13}$$

$$V_{scale}(\hat{x}) = \arg\max_r \Big\{\lambda_2(\hat{x}, r)\Big\}, \tag{14}$$

$\tilde{\lambda}_1$ and $\tilde{\lambda}_2$ are the values of λ_1 and λ_2 at the optimal scales, respectively. Also $\tilde{\mathbf{v}}_1$ and $\tilde{\mathbf{v}}_2$ are defined similarly to $\tilde{\lambda}_1$ and $\tilde{\lambda}_2$. The optimal scale at point $\hat{x} \in \hat{\Omega}$ can be computed from equation (14). Based on the definitions above, we now define the penalty components H_c and H_d as:

$$H_c(\hat{x}) = e^{h_c \times |V_{ness}(\hat{x}) - V_{ness}(\hat{p})|}, \quad \hat{x}, \hat{p} \in \Omega, \tag{15}$$

where h_c is a positive constant and $\hat{p}$ is the initial source point provided by the user. H_d can be represented as

$$H_d(\hat{x}) = e^{h_d \times |V_{ness}(\hat{x}) - V_{ness}(\hat{z})|}, \quad \hat{x}, \hat{z} \in \Omega, \tag{16}$$

where $\hat{z}$ is a point at the minimal path $\gamma_{\hat{x},\hat{p}}$. In the following, we consider a point $\hat{z}$ as *back-tracked* point of $\hat{x}$ if $z \in \gamma_{\hat{x},\hat{p}}$. Let $\gamma_{\hat{x},\hat{z}}$ be a part of $\gamma_{\hat{x},\hat{p}}$ and the length of $\gamma_{\hat{x},\hat{z}}$ in pixel is set to l (*back-tracked length*), then $H_d(\hat{x})$ measures the local intensities consistency along the minimal path $\gamma_{\hat{x},\hat{z}}$.

In contrast, $H_c(\hat{x})$ only depends on the current point $\hat{x}$ and the initial point $\hat{p}$. Using (12), we can see that the FM propagation will travel faster along the pixels which share similar intensities with the *back-tracked* point and $\hat{p}$.

The reason of using 2D FM instead of 2D+radius in the first stage can be explained as: due to the inhomogeneities of retinal vessel gray level and noises, the extracted minimal paths using the proposed metric defined in (11) are not always at the exact centrelines of the vessels. We show this centreline bias in Fig. 2. In most parts of the vessels shown in the second column of Fig. 2, the red dash lines are at the exact centrelines of the vessels except two parts indicated by red arrows in the 3rd and 4th columns. In order to get the accurate extraction results, we have to refine the results from the first stage. In this paper, for the second stage, only the extracted centrelines are necessary.

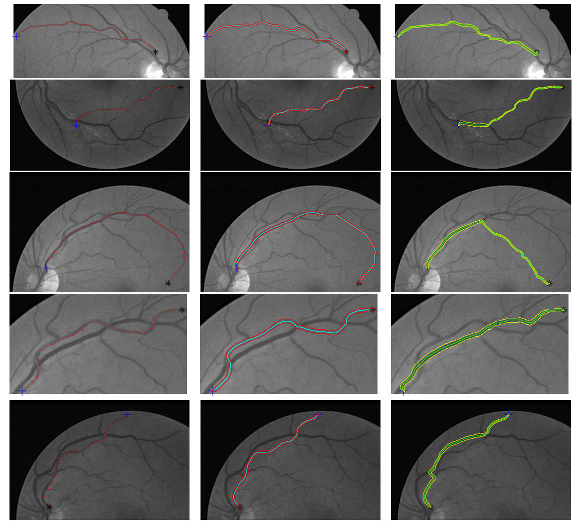

Fig. 3. Demonstration of more results (see text).

B. Centrelines Refinement and Boundaries Extraction

In this section, the centrelines from the first stage can be taken as the prior knowledges. The second stage relies on the B-C model [1]. To overcome centreline bias problem of the first stage, a novel constrained 2D+radius Riemannian metric based on the prior centreline is constructed.

Suppose that the prior centreline obtained from the first stage is denoted as a 2D curve $\hbar$. We introduce a constrained function $D_\hbar$: $\Omega \to R^+, \Omega = \hat{\Omega} \times]R_{min}, R_{max}[$ as:

$$D_\hbar(\mathbf{x}) = \begin{cases} 1, & \text{if } d_\hbar(\mathbf{x}) \le T; \\ +\infty, & \text{else} \end{cases}, \tag{17}$$

where T is a positive constant and we have $T = 4$ in this paper. $d_\hbar$: $\mathbf{\Omega} \to R^+$ is a distance function:

$$d_\hbar(\hat{x}, r) = \min_{\hat{x}_\hbar \in \hbar} \|\hat{x} - \hat{x}_\hbar\|_2. \tag{18}$$

where $\mathbf{x} = (\hat{x}, r)$. Note that function $D_\hbar$ defines an offset region $\mathcal{R}$ in the domain $\mathbf{\Omega}$, inside which the value of $D_\hbar$ is 1 and outside is $+\infty$. Based on equations (6), (17) and (18), we can construct the constrained Riemannian Metric for $\hbar$:

$$\mathcal{M}_\hbar = \begin{pmatrix} (D_\hbar \cdot \tilde{\mathcal{M}}) & \mathbf{0} \\ \mathbf{0} & (D_\hbar \cdot \mathcal{P}_r) \end{pmatrix}. \tag{19}$$

Equ. (19) is the proposed constrained Riemannian metric. Based on this metric, the FM front will propagate only inside the region defined by $D_\hbar$. And the extracted minimal path is a global minimum of the following energy:

$$l(\gamma(s)) := \int_0^L \sqrt{\gamma'^T(s)\mathcal{M}_\hbar(\gamma(s))\gamma'(s)}\, ds \tag{20}$$

The minimizer of energy (20) is a minimal path inside the region $\mathcal{R}$ defined by the prior centreline. As the prior centreline can avoid *short branches combination* problem and will always choose the correct vessel because of the local intensities consistency. The second stage can be considered as a curve refinement procedure taking the prior centreline as initial curve as shown in Fig. 2. In the second column of

Algorithm 1 *FastMarchingLocalIntensitiesConsistency*

Initialization:

For each point $\hat{x} \in \hat{\Omega}$, set $\mathcal{U}_{\hat{p}}(\hat{x})$=$+\infty$. Set $\mathcal{V}(\hat{x})$=*Trial*. Set $\mathcal{U}(\hat{p})$=0.

Marching Loop:

Find $\hat{x}_m$, the *Trial* point which minimizes $\mathcal{U}_{\hat{p}}$.
if $\hat{x}_m$= $\hat{p}_e$ **then**
  Track the minimal path $\gamma_{\hat{p}_e,\hat{p}}$.
  Stop the fast marching propagation.
end if
Tag $\hat{x}_m$ as *Accepted*.
Find the *back-tracked* point $\hat{z}$ of $\hat{x}_m$ using path $\gamma_{\hat{x}_m,\hat{p}}$.
for All $\hat{y}$ such that $\hat{x}_m \in S(\hat{y})$ and $\mathcal{V}(\hat{y}) \neq$ *Accepted* **do**
  Calculate the metric $\tilde{\mathcal{M}}_d(\hat{y})$ using the *back-tracked* point $\hat{z}$ and (11), (15), (16).
  Compute $\mathcal{U}_{\rm new}(\hat{y})$ using (10).
  if $\mathcal{U}_{\rm new}(\hat{y}) < \mathcal{U}(\hat{y})$ **then**
    Set $\mathcal{U}(\hat{y}) \leftarrow \mathcal{U}_{\rm new}(\hat{y})$
  end if
end for

Fig. 2, the cyan solid lines are the results (only centreline is shown) extracted by minimizing (20). We can see that they are more accurate than the red dash lines obtained from the first stage (see the 3rd and 4th columns for details). Thanks to the original B-C method [1], we can extract the centrelines and boundaries at the same time. We demonstrate more results in Fig. 3: in the first column are the original images and the centrelines from the first stage indicated by dash red lines. The second column shows the results of our method from the second stage, with cyan solid lines indicating centrelines and red solid lines indicating boundaries. The last column are the results from the B-C model. For the results of our model, *short branches combination* problem has been avoided even for a long vessel crossing another vessel with strong contrast.

IV. Experiments

A. Numerical Implementation

In this section, we discuss the numerical implementation details using AFM method [5] for the first and second stages respectively. In Algorithm 1 given only an initial point s, once the fast marching front meets the endpoint p_e, we stop the propagation (see Algorithm 1). For robustness, we compute H_c and H_d at point x using the mean value of V_{ness} inside the set $\mathcal{B} := \{p \in \Omega, ||p-x||_2 <= 3\}$. For the second stage, we just perform the regular AFM [5] with metric $\tilde{\mathcal{M}}_\hbar$.

B. Evaluation

We evaluate our method on the test set of the DRIVE dataset [10], which includes 20 retinal images. We choose total 110 vessels which start from the optic disk of the retinal images or those cross another vessel. If the extracted minimal path exactly follows the desire vessel, we consider this is a positive extraction (PE), otherwise a negative extraction(NE).

TABLE I
Comparison of our method and B-C model.

Measures	N_T^F	N_F^T	N_T^T	N_F^F
Number	47	2	55	6

And for our method, the number of $PE = 102$ out of total 110 vessels. For B-C model, the number is 57. Additionally, we compute the following measures: 1) N_F^T: the number of vessels that our method positively extracts and the B-C model fails. 2) N_T^F: the number of vessels that the B-C model positively extracts and our model fails. 3) N_F^F: the number of vessels that both models fail to extract. 4) N_T^T: the number of vessels that both models positively extract. In Table I, we show the four measures. It can be seen that our model are much better than the B-C model (102 against 57).

V. Conclusion

In this paper, we propose a novel two-stage retinal vessels extraction method based on the AFM and local intensities consistency. In the first stage, the vessel between two given points can be roughly extracted and will avoid *short branches combination* problem because of the dynamic metric. Then this rough centreline is taken as prior curve and refined in the second stage. Experiments show that the proposed method indeed outperform the state-of-the-art B-C model [1].

VI. Acknowledgements

We would like to thank Dr. Jean-Marie Mirebeau for fruitful discussions. This work was partially supported by ANR grant NS-LBR, ANR-13-JS01-0003-01.

References

[1] F. Benmansour and L. D. Cohen, "Tubular Structure Segmentation Based on Minimal Path Method and Anisotropic Enhancement," *IJCV*, vol. 92, no. 2, pp. 192–210, 2011.

[2] G. Peyré, M. Péchaud, R. Keriven, and L. D. Cohen, "Geodesic Methods in Computer Vision and Graphics," *Foundations and Trends in Computer Graphics and Vision*, pp. 197–397, 2010.

[3] L. D. Cohen and R. Kimmel, "Global minimum for active contour models: A minimal path approach," *IJCV*, vol. 24, no. 1, pp. 57–78, 1997.

[4] J. A. Sethian, "Fast marching methods," *SIAM Review*, vol. 41, no. 2, pp. 199–235, 1999.

[5] Jean-Marie Mirebeau, "Anisotropic Fast-marching on Cartesian Grids Using Lattice Basis Reduction," *SIAM Journal on Numerical Analysis*, vol. 52, no. 4, pp. 1573–1599, 2014.

[6] H. Li and A. Yezzi, "Vessels as 4-D curves: Global minimal 4-D paths to extract 3-D tubular surfaces and centrelines," *IEEE Transactions on Medical Imaging*, vol. 26, no. 9, pp. 1213–1223, 2007.

[7] Wei Liao, Karl Rohr, and Stefan Wörz, "Globally Optimal Curvature-Regularized Fast Marching For Vessel Segmentation," *MICCAI 2013*, pp. 550–557, 2013.

[8] Max W. K. Law and Albert C. S. Chung, "Three Dimensional Curvilinear Structure Detection Using Optimally Oriented Flux," *Computer Vision-ECCV 2008. Springer Berlin Heidelberg*, pp. 368–382, 2008.

[9] J. N. Tsitsiklis, "Efficient algorithms for globally optimal trajectories," *IEEE Transactions on Automatic Control*, vol. 40, no. 9, pp. 1528–1538, 1995.

[10] J. Staal, M. D Abrámoff, M. Niemeijer, M. A Viergever, and G. Bram, "Ridge-based vessel segmentation in color images of the retina," *IEEE Transactions on Medical Imaging*, vol. 23, no. 4, pp. 501–509, 2004.